Vibronic Relaxation among the Clements Bands of SO_2 from the E-Band Excitation

S. C. Bae, H. S. Son, G. H. Kim, and J. K. Ku*

Department of Chemistry, Pohang University of Science and Technology, Pohang, Kyung-buk, 790-784, South Korea

Received: February 3, 1999; In Final Form: May 24, 1999

Vibronic relaxation among the Clements bands of SO_2 molecule has been studied from time-resolved fluorescence spectra in the 300−350 nm region. The $K' = 6$, $J' = 7$ level of the Clements E-band was populated at 32 812.8 cm^{-1}, and detailed time-resolved fluorescence spectra for the period 0−160 ns were obtained. Following the fast decay of the laser excited level, weak emissions from Clements A−F bands appeared almost simultaneously. The simultaneous appearance of many Clements bands was attributed to fast rovibronic relaxation of the laser excited molecules among the dark levels. It was also found that the broad apparent continuum emission following the direct fluorescence showed different decay rates at different wavelengths, but the decay rates of the emissions for $\lambda > 350$ nm were virtually identical. Based on the wavelength dependence of the decay rates, the apparent continuum emissions were ascribed to the emissions from the rovibronically dispersed hybrid bright states and the low-lying rovibrational levels of the $\tilde{A}^1A_2$ state generated by collisional relaxation of the laser-excited level.

1. Introduction

The absorption bands of the SO_2 molecule in the 260−315 nm region, named Clements bands, have been extensively studied by many research groups because of the intrinsic interest in the sophisticated interactions among those nearby excited states as well as the practical importance in atmospheric chemistry.[1,2] The rotational analyses and the Franck−Condon studies have shown that all the Clements bands belong to the $\tilde{A}^1A_2 \leftarrow \tilde{X}^1A_1$ transition and that they are essentially hybrid vibronic states resulting from strong vibronic coupling between the $\tilde{A}^1A_2$ and $\tilde{B}^1B_1$ states.[3−6] Besides, the Clements bands region of the $\tilde{A}^1A_2$ state is strongly perturbed by spin−orbit coupling with nearby triplet states and by Coriolis coupling with the high-lying vibrational levels of the ground state.[7−9] While the spectroscopic properties of the Clements bands are reasonably well understood, the kinetic behaviors, especially on the vibronic relaxation among the Clements bands, are not well characterized yet.

In the previous work,[10] we have reported time-resolved emission spectra from both the E-band and $\tilde{A}^1A_2(0,8,1)$ level excitation and proposed the following relaxation mechanism for the E-band excitation.

$$^1A_1 + h\nu \rightarrow H(^1A_2^n + {}^1B_1^n) \quad (1)$$

$$H(^1A_2^n + {}^1B_1^n) \rightarrow {}^1A_1 + h\nu_{1f}\,(\text{direct emission}) \quad (2)$$

$$H(^1A_2^n + {}^1B_1^n) + M \rightarrow {}^3B_1^m + M \quad (3)$$

$$H(^1A_2^n + {}^1B_1^n) + M \rightarrow H(^1A_2^{n'} + {}^1B_1^{n'}) + M \quad (4)$$

$$^3B_1^m + M \rightarrow H(^1A_2^{n'} + {}^1B_1^{n'}) + M \quad (5)$$

$$H(^1A_2^{n'} + {}^1B_1^{n'}) \rightarrow {}^1A_1 + h\nu_{2f}\,(\text{continuum emission}) \quad (6)$$

$$^3B_1^m + M \rightarrow {}^3B_1^{0,1} + M \quad (7)$$

$$^3B_1^{0,1} \rightarrow {}^1A_1 + h\nu_p(\text{phosphorescence}) \quad (8)$$

$H(^1A_2^n + {}^1B_1^n)$ represents a hybrid level derived from the $\tilde{A}^1A_2$ and $\tilde{B}^1B_1$ vibronic levels, that is, the Clements bands; the superscripts n, n', and m refer to the vibrationally excited levels, and $^3B_1^{0,1}$ is the low-lying vibrational levels ($v = 0$ and 1) of the $\tilde{a}^3B_1$ state. The time-resolved spectra reported in the previous work clearly show the direct fluorescence from the E-band at early time, the phosphorescence from the low-lying vibrational levels of the $\tilde{a}^3B_1$ state at later time, and a broad apparent continuum emission appearing at intermediate time.

The above kinetic scheme explains the previous results qualitatively well. Moreover, eqs 3−6 corresponding to the initial steps of the collisional processes are consistent with the kinetic scheme proposed by Koda and co-workers.[11] However, the time-resolved spectra taken with 100 ns or longer time intervals did not show discernible features for vibronic relaxation among the Clements bands due to the appearance of the relatively strong overlapping apparent continuum emission. The present work focuses on the features of the vibronic relaxation among the Clements bands and resolves these features by exciting the $K' = 6$, $J' = 7$ level of the Clements E-band of the SO_2 molecule. When the time-resolved fluorescence spectra were taken with much shorter time intervals, emissions from the nearby and lower-lying Clements bands were observed. In addition, the fluorescence decay rates of the apparent continuum emission were investigated at various wavelengths to obtain additional information about the nature of the emitting species.

2. Experimental Section

Details of the experimental setup have been described elsewhere.[10] In brief, a Q-switched Nd:YAG pumped dye laser (Quantel YG681-TDL60) was used as an excitation source. The pulse duration of the frequency-doubled dye laser beam was about 8 ns, and the spectral bandwidth was less than 0.1 cm^{-1} at 32 812.8 cm^{-1}. The fluorescence gas cell was made of a 2 L Pyrex bulb, and two pairs of 1 in. (2.54 cm) Pyrex O-ring joints were attached to allow for the windows of the laser beam path and for the connection to the gas handling vacuum rack. The

10.1021/jp990390f CCC: $18.00
Published on Web 08/31/1999

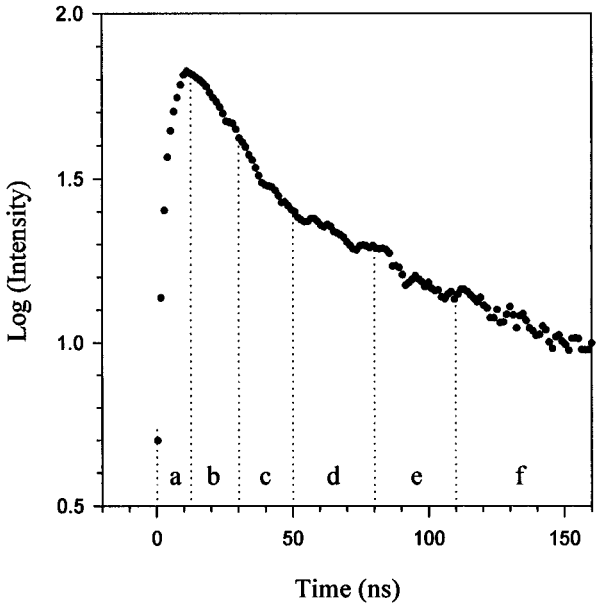

Figure 1. A typical emission time profile from $K' = 6$, $J' = 7$ level of E-band excitation at 1.0 Torr of pure SO_2. The laser wavelength was set at 32 812.8 cm^{-1}, and the fluorescence was monitored at 309.4 nm where the E-band $\rightarrow \tilde{X}^1A_1(0,1,0)$ transition.

fluorescence from the excited molecules was monitored at a perpendicular direction from the laser beam path through a 2 in. quartz window attached to the bulb with a short arm. Time-resolved emission spectra were obtained from time profiles collected at each wavelength by scanning a 0.5 m monochromator (Spex 500M) equipped with a cooled Hamamatsu R928 photomultiplier tube (PMT). The signal from the PMT was transferred to a digitizing oscilloscope (Tektronix TDS520) interfaced to a laboratory computer for signal averaging and processing. Emissions from 500 laser pulses were accumulated to get one time profile at the given wavelength. The time profile was divided into several time intervals, and all the digitized signals in each interval were summed and stored separately before scanning the monochromator to the next wavelength. The SO_2 gas with 99.98% purity was purchased from Matheson, and further purified by a freeze−pump−thaw method on the vacuum rack. An oil manometer was used to measure the cell pressure above 0.5 Torr, while a convectron gauge (Granville-Phillips 307) was used to measure lower pressures.

3. Results and Discussion

A typical fluorescence time profile for 0−160 ns following the $K' = 6$, $J' = 7$ level of the E-band excitation at 1.0 Torr of SO_2 is shown in Figure 1. The $K' = 6$ and $J' = 7$ level of the E-band located at 32 812.8 cm^{-1} is known to be less crowded than other rovibronic levels in the E-band.[4,12] Though the fluorescence from the first excited singlet state was observed for ~1 μs at 1.0 Torr of SO_2, the time profile was taken for 0−160 ns following the laser excitation to investigate the kinetics of depletion of the laser excited level in early time. The time profile clearly displays two exponentially decaying components. The time profile was arbitrarily divided into six parts, as shown in Figure 1, to obtain time-resolved spectra. The time-resolved spectra shown in Figure 2 were obtained from the E-band excitation at 1.0 Torr of pure SO_2 in the 300−350 nm range. It has been previously shown that emission from the $\tilde{a}^3B_1$ state appears with time delay greater than 1.2 μs and lasts more than 10 μs at 1.0 Torr of SO_2 following the E-band excitation. Details of overall time-resolved emission spectra for

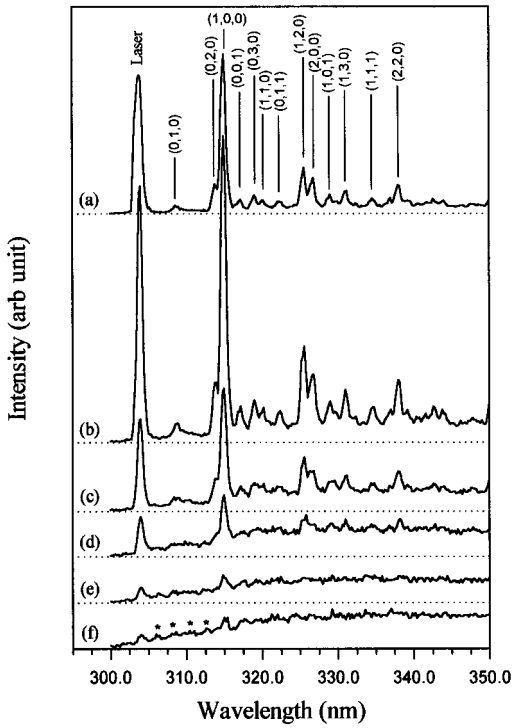

Figure 2. Time-resolved emission spectra obtained from the E-band excitation at 1.0 Torr of pure SO_2 for (a) 0−12.5, (b) 12.5−30, (c) 30−50, (d) 50−80, (e) 80−120, and (f) 120−160 ns periods. The $K' = 6$ and $J' = 7$ level of the E-band was excited at 32 812.8 cm^{-1}. The assignments given in (a) correspond to the E-band $\rightarrow \tilde{X}^1A_1(n_1,n_2,n_3)$ transitions.

a longer time period (0−9 μs) have been reported in the previous work.[10a] As shown in Figure 2a, the characteristic vibrational progressions appear in early time due to the fluorescence from the laser-excited level to the ground electronic state. The intensity of these sharp peaks decays monotonically and the broad continuum emission appears as time elapses. This result agrees well with our previous observation.[10a] However, some weak peaks denoted by asterisks in Figure 2f appeared with a regular spacing on top of the apparent continuum emission in the 300−315 nm region. Their peak wavelengths are different from those shown in Figure 2a.

To more closely examine the time evolution of the emission peaks, we obtained detailed time-resolved fluorescence spectra for 0−160 ns with 4 ns time intervals in the 300−315 nm range. This spectral region is chosen because there are only three vibronic transitions from the laser excited level in this region as shown in Figure 2a. The results are plotted in Figure 3. It is evident that the emission peaks from the laser excited level decrease monotonically and that new emission peaks appear almost simultaneously as time elapses, even though their peak intensities are weak. When compared with the absorption spectra reported by Clements,[13] the locations and the spacing of those new emission peaks in the 300−315 nm region match well with those of Clements A−F bands as labeled in Figure 3. To confirm that these weak emissions result from those Clements A−F bands $\rightarrow \tilde{X}^1A_1(0,0,0)$ transitions and to look for the appearance of these emissions at different rovibronic level excitation, we also investigated time-resolved spectra in the 300−330 nm region by exciting at three different wavelengths. Figure 4 shows emission spectra taken for a 100−200 ns time period following the laser excitation at 32 812.8 cm^{-1} [$^PP_7(8)$], 32 811.2 cm^{-1} [$^PP_7(11)$], and 32 818.0 cm^{-1} [$^PQ_7(8)$], respectively. They look very similar in showing both Clements A−F bands $\tilde{X}^1A_1(0,0,0)$ emissions in the 300−314 nm range and Clements A−E

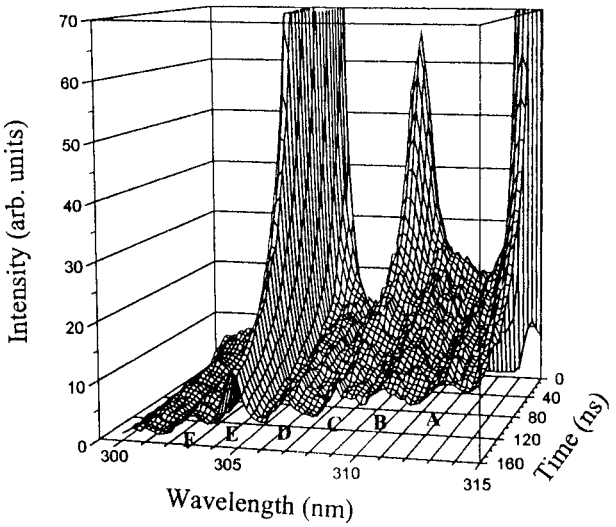

Figure 3. Three-dimensional view of the detailed time-resolved emission spectra from the E-band excitation at 1.0 Torr of pure SO_2. The time-resolved spectra were taken at 4 ns intervals for 0−160 ns after the laser excitation. The peaks denoted by letters in the figure represents emissions from the corresponding Clements bands → $\tilde{X}^1A_1(0,0,0)$ transitions.

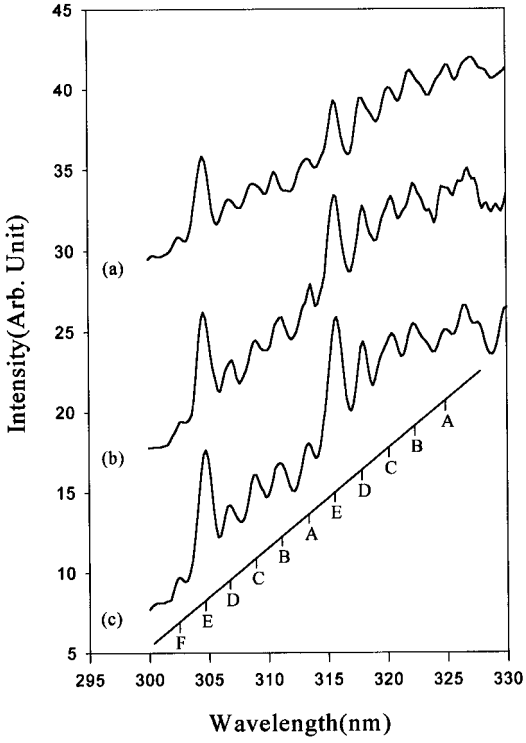

Figure 4. Emission spectra in the 300−330 nm region at 1.0 Torr of SO_2. The spectra were taken for 100−200 ns time period following the laser excitation at (a) 32 812.8 cm^{-1} [$^PP_7(8)$], (b) 32 811.2 cm^{-1} [$^PP_7(11)$], and (c) 32 818.0 cm^{-1} [$^PQ_7(8)$], respectively. Clements A−F bands $\tilde{X}^1A_1(0,0,0)$ and Clements A−E bands $\tilde{X}^1A_1(1,0,0)$ emissions are shown.

bands → $\tilde{X}^1A_1(1,0,0)$ emissions in the 315−325 nm region. Figures 3 and 4 show the vibronic relaxation among the Clements bands.

Until now, there are only a few reports on the vibronic relaxation in the first excited singlet state of SO_2. Mettee[14] has studied the pressure and exciting wavelength dependence of the emission spectra. He investigated emission spectra from six Clements bands using a Hg−Xe lamp as an excitation source and observed some vibronic relaxation when the higher-lying Clements bands were excited. He concluded that the vibronic relaxation would occur with a cross section near the gas kinetic value (2.6×10^{-10} cm^3 $molecule^{-1}$ s^{-1}). Holtermann et al.[12b] mentioned that collision-induced vibronic relaxation among the Clements bands should be very ineffective compared to collision-induced electronic quenching. However, a closer examination of the pressure dependence of the fluorescence spectra reported by Holtermann et al.[12a] reveals that some new emission peaks appear in the 304.7−315.0 nm region at 34 mTorr of pure SO_2 while those weak emission peaks do not appear at 0.7 mTorr. Comparing the spectra reported by Holtermann et al.[12a] with Figure 3, it is evident that those unassigned weak peaks at 34 mTorr come from the Clements D-, B-, and A-band, and that the E-band → $\tilde{X}^1A_1(0,1,0)$ emission overlaps with the C-band emission. Shaw and co-workers[15] have reported single vibronic level fluorescence spectra of SO_2 from Clements D-, E-, F-, and G-band excitation. Their fluorescence spectra also contain emission peaks from vibronically relaxed Clements bands. Koda and co-workers[12] have studied collisional relaxation of several rovibronically selected levels in the Clements E-band in a supersonic jet. They observed that fluorescence time profiles deviated from the single-exponential decay, but they could not resolve detailed features for vibronic relaxation among the Clements bands. Hegazi and co-workers[16] have shown that the low-lying vibrational levels of the $\tilde{A}^1A_2$ state result from the collision-induced vibronic relaxation from the Clements F- and E-band excitations. However, they could not observe the emissions from the lower-lying Clements bands derived from the vibronic relaxation among the Clements bands. Thus, the collision-induced vibronic relaxation among the Clements bands has been observed by Mettee,[3] Holtermann et al.,[12a] and Shaw et al.[15]

Figure 3 shows that Clements A−F bands appear almost simultaneously and that the emission intensities are very weak. Considering the energy separation between the adjacent Clements bands is about 230 cm^{-1}, the simultaneous appearance of those weak Clements bands suggests that these bands may be populated dominantly from dark levels, because the density of dark levels in this energy region is much higher than that of bright levels. The bright levels mean those hybrid vibronic levels between the $\tilde{A}^1A_2$ and $\tilde{B}^1B_1$ states that emit fluorescence, and the dark levels include triplet states ($\tilde{a}^3B_1$, $\tilde{b}^3A_2$, and $\tilde{c}^3B_2$)[20] in addition to the hybrid vibronic levels between the $\tilde{A}^1A_2$ and $\tilde{B}^1B_1$ states that do not emit fluorescence. In fact, the collisional self-quenching rate constant for the laser excited level is very large as shown in Figure 5, where the pressure dependence of the fast and slow component decay rates from the $K' = 6$, $J' = 7$ level of the E-band excitation is plotted. The radiative lifetime and self-quenching rate constant for the laser excited level are 14.6 ± 0.3 μs and (2.2 ± 0.2) × 10^{-9} cm^3 $molecule^{-1}$ s^{-1}, respectively, from the low-pressure data. These values are in good agreement with those of Holtermann et al.[12a] However, the apparent self-quenching rate constant at higher pressures (above 2.0 Torr) are (9.2 ± 0.8) × 10^{-10} and (3.3 ± 0.4) × 10^{-10} cm^3 $molecule^{-1}$ s^{-1} for the fast and slow components, respectively, as plotted in Figure 5b. The apparent self-quenching rate constant for the fast component at higher pressures is about 2.4 times less than the corresponding value at low pressures. This change of apparent self-quenching rate constants on different pressure ranges has been studied for the phosphorescence emission ($\tilde{a}^3B_1 \rightarrow \tilde{X}^1A_1$) of SO_2,[17−19] but the pressure saturation of fluorescence quenching of the hybrid singlet state is observed at much lower pressures due to extensive collisional mixing in this energy region. The apparent

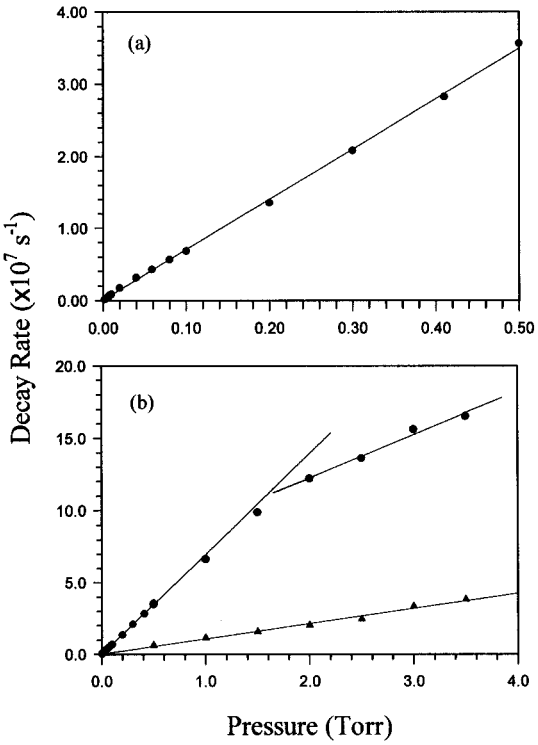

Figure 5. Pressure dependence of decay frequencies for the emission from $K' = 6$, $J' = 7$ level of E-band excitation: (a) 0−500 mTorr (●) and (b) 0.5−4.0 Torr range for fast (●) and slow (▲) component. The fluorescence for the E-band → $\tilde{X}^1A_1(0,1,0)$ emission was monitored at 315.8 nm. The radiative lifetime and collisional self-quenching rate constant from low-pressure plot are 14.5 ± 0.3 μs and (2.2 ± 0.2) × 10^{-9} cm^3 molecule^{-1} s^{-1}.

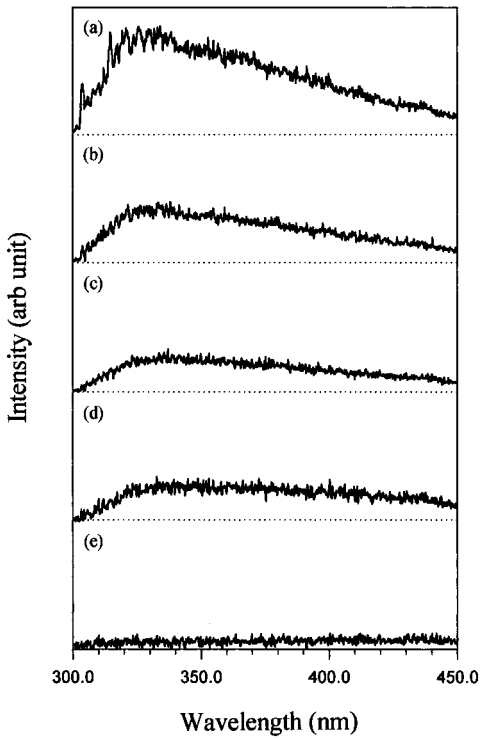

Figure 6. Time-resolved emission spectra of the continuum emission for 100−1200 ns period at 1.0 Torr of pure SO_2: (a) 100−200 ns, (b) 200−300 ns, (c) 300−400 ns, (d) 400−800 ns, and (e) 800−1200 ns periods.

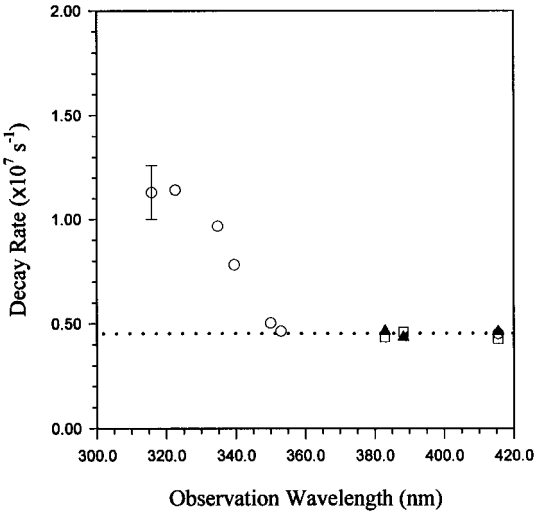

Figure 7. Fluorescence decay rates of the continuum emission at various wavelengths. All the fluorescence decay rates were obtained at 1.0 Torr of pure SO_2, and the time zone for the decay analysis was fixed for 200−800 ns period in which the continuum emission is dominant. Three vibronic bands were excited: E-band (●), B-band (■), and $\tilde{A}^1A_2(0,8,1)$ (▲).

self-quenching rate constant obtained from Stern−Volmer plot at low pressures must be the sum of electronic quenching and rovibronic relaxation rate constants among those bright and dark levels. Since the density of dark levels is much larger than that of bright ones, the dominant relaxation process is expected to be the dark level formation and major fractions of the apparent quenching rate constant should be assigned to this process. At higher pressures, the apparent quenching rate constant of the fast component exhibits pressure saturation and it is difficult to refer to simple processes. However, the apparent quenching rate constant of the slow component could be related to overall quenching processes of the dark levels, including vibrational relaxation in the $\tilde{a}^3B_1$ state, assuming that the collisional coupling between the bright and dark levels is strong. We attempted to estimate the magnitude of the collision-induced vibronic relaxation among the Clements bands, but it was unsuccessful due to the complicated role of the dark levels in this energy region.

Likewise, time-resolved emission spectra and fluorescence decay rates of the apparent continuum emission were monitored at 1.0 Torr of pure SO_2. These apparent continuum emission may originate from spectral congestion due to the fast collisional relaxation among the excited levels. Figure 6 shows the time evolution of the apparent continuum emission spectra for the 100−1200 ns period at 1.0 Torr of pure SO_2. The intensity of the broad continuum emission decreases monotonically and the shape of the continuum slightly changes with time. At early time, the broad emission shows an intensity maximum at ∼330 nm with a red-shaded form. The shape of the continuum emission becomes flat at later time, as shown in Figure 6, d and e. These changes of the shape of continuum emission suggest that there may be more than two emitting species involved in the continuum emission. To get additional information about the nature of the emitting species contributing to the continuum emission, we have measured the fluorescence decay rates at various emission wavelengths and plotted in Figure 7. All the emissions are observed at 1.0 Torr of pure SO_2, and the decay rates are obtained by analyzing the time profiles for a 200−800 ns period in which the continuum emission is dominant. As shown in Figure 7, the fluorescence decay rates for the emissions in the 300−350 nm region decrease with increasing wavelength and the decay rates of the emissions for $\lambda > 350$ nm are almost identical. This result suggests that the

continuum emission arises from at least two components: those relatively fast decaying species for $\lambda < 350$ nm and those slow decaying species for $\lambda > 350$ nm. The average decay rate of the slow component appeared in $\lambda > 350$ nm is $(4.5 \pm 0.2) \times 10^6$ s^{-1}, as denoted by a dotted line in Figure 7. Since the radiative lifetimes of the first excited singlet state SO_2 molecules are in the 10−600 μs range,[12,21] the radiative decay rate for the continuum emission should be less than 1×10^5 s^{-1}. Neglecting this radiative decay rate allows the estimation of the collisional quenching rate constant of the continuum emission. A value of $(1.4 \pm 0.1) \times 10^{-10}$ cm^3 $molecule^{-1}$ s^{-1} is obtained from the average decay rate of the continuum emission for $\lambda > 350$ nm. This value matches well with the previously reported quenching rate constant, $(1.5 \pm 0.1) \times 10^{-10}$ cm^3 $molecule^{-1}$ s^{-1}, for the slow component from the excitation of (0,4,1) and (1,2,1) vibrational levels of the $\tilde{A}^1A_2$ state within error limits.[10b] Thus, the emitting species responsible for the apparent continuum emission for $\lambda > 350$ nm seems to be the low-lying vibrational levels of the $\tilde{A}^1A_2$ state produced by the collision-induced vibronic relaxation from the Clements bands. On the other hand, the emitting species for the fairly fast decaying emissions for $\lambda < 350$ nm appears to be the bright hybrid levels between the $\tilde{A}^1A_2$ and $\tilde{B}^1B_1$ states which locate above the origin of the $\tilde{B}^1B_1$ state. The fast decay rates for these species could be attributed to the dense rovibronic levels in this energy region which contribute to the electronic quenching including intersystem crossing.

4. Conclusion

The observation of the simultaneous appearance of the Clements A−F bands following the Clements E-band excitation provides useful information about the vibronic relaxation among the Clements band. Based on this observation, the kinetic scheme given in eqs 1−8 is modified to include the dark levels and the vibronic relaxation among the Clements bands. To accommodate the dark levels to the kinetic scheme, eqs 3−7 need to be replaced by eqs 9−13.

$$H(^1A_2^n + {}^1B_1^n) + M \rightarrow D(\text{dark levels}) + M \quad (9)$$

$$\rightarrow H(^1A_2^{n'} + {}^1B_1^{n'}; \text{bright levels}) + M \quad (10)$$

$$D(\text{dark levels}) + M \rightarrow H(^1A_2^{n'} + {}^1B_1^{n'}; \text{bright levels}) + M \quad (11)$$

$$D(\text{dark levels}) + M \rightarrow {}^3B_1^{0,1} + M \quad (12)$$

$$H(^1A_2^{n'} + {}^1B_1^{n'}; \text{bright levels}) \rightarrow {}^1A_1 + h\nu_{2f}(\text{Clements}) \quad (13)$$

D(dark levels) includes all the nonemitting interacting levels, such as $^3B_1^m$, $^3A_2$, $^3B_2$, and nonemitting levels of $H(^1A_2^{n'} + {}^1B_1^{n'})$. Also, the wavelength dependence of decay rates of the apparent continuum emission suggests that the processes given by eqs 14−16 take place in the vibronic relaxation of Clements bands.

$$H(^1A_2^{n'} + {}^1B_1^{n'}; \text{bright levels}) + M \rightarrow {}^1A_2(\text{low } v) \quad (14)$$

$$D(\text{dark levels}) + M \rightarrow {}^1A_2(\text{low } v) + M \quad (15)$$

$$^1A_2(\text{low } v; \text{bright levels}) \rightarrow {}^1A_1 + h\nu_{3f}(\text{continuum}) \quad (16)$$

Although the above kinetic scheme is derived from excitation of the $K' = 6$, $J' = 7$ level of the Clements E-band, it should also be applicable to other rovibronic level excitation in the Clements band.

Acknowledgment. This work is financially supported in part by the Korea Science and Engineering Foundation through the Center of Molecular Science at KAIST and in part by the Ministry of Education through the Basic Research Institute Program (BSRI-97-3438).

References and Notes

(1) Heicklen, J.; Kelly, N.; Partymiller, K. *Rev. Chem. Intermed.* **1980**, *3*, 315 and references therein.
(2) Heicklen, J. *Atmospheric Chemistry*; Academic Press: New York, 1976.
(3) Hamada, Y.; Merer, A. J. *Can. J. Phys.* **1974**, *52*, 1443.
(4) Hamada, Y.; Merer, A. J. *Can. J. Phys.* **1975**, *53*, 2555.
(5) Shaw, R. J.; Kent, J. E.; O'Dwyer, M. F. *J. Mol. Spectrosc.* **1980**, *82*, 1.
(6) Kullmer, R.; Demtröder, W. *Chem. Phys.* **1985**, *92*, 423.
(7) Kullmer, R.; Demtröder, W. *J. Chem. Phys.* **1985**, *83*, 2712.
(8) Watanabe, H.; Tsuchiya, S.; Koda, S. *J. Chem. Phys.* **1985**, *82*, 5310.
(9) Suzuki, T.; Ebata, T.; Ito, M.; Mikami, N. *Chem. Phys. Lett.* **1985**, *126*, 268.
(10) (a) Bae, S. C.; Kim, G. H.; Ku, J. K. *Chem. Phys. Lett.* **1997**, *265*, 385. (b) Bae, S. C.; Yoo, H. S.; Ku, J. K. *J. Chem. Phys.* **1998**, *109*, 1251. (c) Bae, S. C.; Lee, K.; Kim, G. H.; Ku, J. K. *J. Chem. Phys.* **1995**, *102*, 1665.
(11) Koda, S.; Yamada H.; Tsuchiya S. *J. Phys. Chem.* **1988**, *92*, 383.
(12) (a) Holtermann, D. L.; Lee, E. K. C.; Nanes, R. *J. Phys. Chem.* **1983**, *87*, 3926. (b) Holtermann, D. L.; Lee, E. K. C.; Nanes, R. *J. Chem. Phys.* **1982**, *77*, 5327.
(13) Clements, J. H. *Phys. Rev.* **1935**, *47*, 224.
(14) Mettee, H. D. *J. Chem. Phys.* **1968**, *49*, 1784.
(15) Shaw, R. J.; Kent, J. E.; O'Dwyer, M. F. *Chem. Phys.* **1976**, *18*, 165; 155.
(16) Hegazi, E.; Al-Adel, F.; Hamdan, A.; Dastageer, A. *J. Phys. Chem.* **1994**, *98*, 12169.
(17) (a) Strickler, S. J.; Rudolph, R. N. *J. Am. Chem. Soc.* **1978**, *100*, 3326. (b) Strickler, S. J.; Ito, R. D. *J. Phys. Chem.* **1985**, *89*, 2366.
(18) Su, F.; Wampler, F. B.; Bottenheim, J. W.; Thorsell, D. L.; Calvert, J. G.; Damon, E. K. *Chem. Phys. Lett.* **1977**, *51*, 150.
(19) Bae, S. C.; Lee, S. R.; Ku, J. K. *Bull. Korean Chem. Soc.* **1996**, *17*, 56.
(20) Kamiya, K.; Matsui, H. *Bull. Chem. Soc. Jpn.* **1991**, *64*, 2792.
(21) Brus, L. E.; McDonald, J. R. *J. Chem. Phys.* **1974**, *61*, 97.